HHS Public Access

Author manuscript

Neuroimage. Author manuscript; available in PMC 2018 February 01.

Published in final edited form as:

Neuroimage. 2017 February 01; 146: 1050–1061. doi:10.1016/j.neuroimage.2016.10.049.

Functional circuit mapping of striatal output nuclei using simultaneous deep brain stimulation and fMRI

Nathalie Van Den Berge[1,2,5,1], **Daniel L. Albaugh**[1,2,3,1], **Andrew Salzwedel**[7], **Christian Vanhove**[5], **Roel Van Holen**[5], **Wei Gao**[7], **Garret D. Stuber**[3,5], and **Yen-Yu Ian Shih**[1,2,3,4,*]

[1]Department of Neurology, University of North Carolina, Chapel Hill, NC, USA

[2]Biomedical Research Imaging Center, University of North Carolina, Chapel Hill, NC, USA

[3]Curriculum in Neurobiology, University of North Carolina, Chapel Hill, NC, USA

[4]Department of Biomedical Engineering, University of North Carolina, Chapel Hill, NC, USA

[5]Medical Image and Signal Processing Group, Ghent University, Ghent, BELGIUM

[6]Department of Psychiatry, University of North Carolina, Chapel Hill, NC, USA

[7]Biomedical Imaging Research Institute, Department of Biomedical Sciences and Imaging, Cedars-Sinai Medical Center, Los Angeles, CA, USA

Abstract

The substantia nigra pars reticulata (SNr) and external globus pallidus (GPe) constitute the two major output targets of the rodent striatum. Both the SNr and GPe converge upon thalamic relay nuclei (directly or indirectly, respectively), and are traditionally modeled as functionally antagonistic relay inputs. However, recent anatomical and functional studies have identified unanticipated circuit connectivity in both the SNr and GPe, demonstrating their potential as far more than relay nuclei. In the present study, we employed simultaneous deep brain stimulation and functional magnetic resonance imaging (DBS-fMRI) with cerebral blood volume (CBV) measurements to functionally and unbiasedly map the circuit- and network level connectivity of the SNr and GPe. Sprague-Dawley rats were implanted with a custom-made MR-compatible stimulating electrode in the right SNr ($n = 6$) or GPe ($n = 7$). SNr- and GPe-DBS, conducted across a wide range of stimulation frequencies, revealed a number of surprising evoked responses, including unexpected CBV decreases within the striatum during DBS at either target, as well as GPe-DBS-evoked positive modulation of frontal cortex. Functional connectivity MRI revealed global modulation of neural networks during DBS at either target, sensitive to stimulation frequency and readily reversed following cessation of stimulation. This work thus contributes to a

*Correspondence: Yen-Yu Ian Shih, Ph.D., Experimental Neuroimaging Laboratory, Department of Neurology and Biomedical Research Imaging Center, 125 Mason Farm Road, CB# 7513, University of North Carolina, Chapel Hill, NC 27599, Tel: +919 843 4729, Fax: +919 843 4456. shihy@unc.edu.

[1]These authors contributed equally to this work.

growing literature demonstrating extensive and unanticipated functional connectivity among basal ganglia nuclei.

Graphical abstract

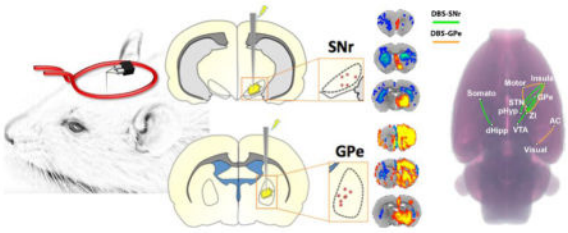

Keywords

Deep brain stimulation; fMRI; external globus pallidus; substantia nigra pars reticulata; striatum; rat

1 Introduction

The striatum represents the major input nucleus of the basal ganglia, critical for the processing and regulation of motor, cognitive, and limbic functions. Striatal output pathways within the basal ganglia are classified as “direct” or “indirect”, based on neurochemical phenotype and axonal projection patterns. Specifically, direct pathway striatal neurons express the D1 dopamine receptor and project to the substantia nigra pars reticulata (SNr) and/or internal globus pallidus (GPi) (i.e., the canonical basal ganglia outputs), whereas indirect pathway striatal neurons express the D2 dopamine receptor and innervate the external globus pallidus (GPe). Both the direct and indirect pathways ultimately converge upon thalamocortical relays, through direct innervation of the basal ganglia outputs (SNr/GPi), or a polysynaptic route (GPe -> STN), respectively. According to long-upheld models of the basal ganglia, these pathways are functionally antagonistic; the direct pathway activates thalamocortical circuits, whereas the indirect pathway facilitates their suppression (via disinhibition of the SNr/GPi) (Albin et al., 1989; DeLong, 1990).

In recent years, this relatively simplistic framework of direct/indirect pathway function has come under increasing scrutiny (Calabresi et al., 2014; Cui et al., 2013; Friend and Kravitz, 2014; Gittis et al., 2014; Goldberg et al., 2013; Jahfari et al., 2011; Tecuapetla et al., 2014). Although evidence continues to support the notion of functional antagonism between these pathways (Freeze et al., 2013; Kravitz et al., 2010; Schmidt et al., 2013), additional anatomical and functional studies have identified unanticipated circuit connectivity in both the SNr and GPe (among other basal ganglia nuclei). Recent examples in the GPe include the identification of a pallidocortical projection that entirely bypasses thalamic relays to modulate frontal cortex (Chen et al., 2015; Saunders et al., 2015), as well as pallidostriatal innervation by so-called “arkypallidal” GPe neurons (Abdi et al., 2015; Mallet et al., 2012). The SNr, generally conceptualized as an inhibitory nucleus, contains a subset of glutamatergic neurons recently mapped to innervate and excite the reticular thalamus, a higher-order non-relay region (Dunn et al., 2009). The functional roles of these novel circuit

elements are likely complex and not easily predicted. Experimental approaches that allow for the large-scale characterization of functional circuit connections will greatly facilitate our understanding of SNr and GPe connectivity, further elucidating the functional roles of both traditional and newly-established circuits.

Functional magnetic resonance imaging (fMRI) represents a powerful tool to study neural circuit modulation on a global scale. When combined with neural stimulation approaches (e.g., deep brain stimulation; DBS), fMRI allows for the relatively unbiased identification of brain areas functionally interconnected with the stimulation target (Albaugh and Shih, 2014; Canals et al., 2009; Dunn et al., 2009; Knight et al., 2013; Lai et al., 2014; Lee et al., 2010; Ross et al., 2016; Shih et al., 2014b; Shyu et al., 2004; Younce et al., 2014). Electrical DBS is notable as a neural stimulation method for its ability to modulate activity within both inputs and outputs of the target nucleus (the former through antidromic signal propagation), although it does lack cell-type specificity and is also capable of affecting fibers of passage (Kringelbach et al., 2007). In addition to identifying putatively connected areas, DBS-fMRI might also shed light on their functional excitatory and/or inhibitory relationships (based on whether the hemodynamic change is positive or negative). Importantly, both the recruitment of select circuits, as well as the directionality of their fMRI responses, may be strongly contingent upon stimulation frequency. For example, low frequency (10 Hz) electrical stimulation of the ventrolateral thalamus in pigs generated a positive blood-oxygen-level-dependent (BOLD) response in motor cortex, whereas high frequency (130 Hz) stimulation evoked a negative BOLD response in the same region (Paek et al., 2015). Thus, in varying stimulation parameters, DBS-fMRI can shed light on the tuning properties of functionally connected circuits. To our knowledge, neither the SNr nor GPe have previously been studied by DBS-fMRI in humans or animal models, including analyses of stimulation frequency-dependent DBS responses.

In the present study, we employed simultaneous DBS-fMRI in the normal rat to map the functional circuits of the SNr and GPe. These areas represent the major striatal output nuclei of the rat direct and indirect pathways, respectively. Evoked-fMRI revealed cerebral blood volume (CBV) modulation by GPe- or SNr-DBS (conducted at a range of stimulation frequencies) in a diverse complement of both overlapping and distinct brain regions, including convergent and unexpected CBV decreases within striatum, and GPe-DBS-evoked positive modulation of frontal cortex. Functional connectivity, measured with functional connectivity fMRI (fcMRI) (Pawela et al., 2008; Raichle, 2011), was significantly modulated by DBS at either target during high (130 Hz) but not lower frequency (40 Hz) stimulation, occurred preferentially in the ipsilateral hemisphere, and was readily reversed following cessation of stimulation.

2 Materials and Methods

2.1 Subjects

Thirteen adult male Sprague-Dawley rats (300–500 g body weight; Charles River Laboratories, Wilmington, MA, USA) were used in this study. All procedures were performed in accordance with the National Institutes of Health Guidelines for Animal Research (Guide for the Care and Use of Laboratory Animals) and approved by the

University of North Carolina Institutional Animal Care and Use Committee. Animals were housed under environmentally-controlled conditions (12 h normal light/dark cycles, 20–23°C and 40–60% relative humidity), with food and water provided *ad libitum*.

2.2 DBS Electrode Implantation Surgery

Rats were anesthetized using nosecone-supplied isoflurane (1.5–2%), and head-fixed within a stereotaxic frame (Model 962, Kopf Instruments, Tujunga, CA, USA). Following head shaving and exposure of the skull, four small burr holes were drilled: three for the positioning of MR-compatible miniature brass screws (Item #94070A031, McMaster Carr, Atlanta, GA, USA) and one for the insertion of a bipolar DBS electrode. Each electrode was custom-made using two-channel tungsten microelectrodes (A-M Systems, WA, U.S.A.), with a 50 μm diameter (single lead), as previously described (Lai et al., 2015). These electrodes were fully insulated with polyimide except at the tips, and the leads were adhered for direct contact using a saturated sucrose solution. The *in vitro* impedance of these electrodes was previously measured as 18–22 kΩ at 1 kHz (Lai et al., 2015).

Electrodes were implanted targeting either the right SNr or GPe (n = 6 and 7, respectively). Stereotactic implantation coordinates were generated using a standard rat brain atlas (Paxinos and Watson, 2004), and are described as follows, in reference to bregma (anteroposterior, AP; mediolateral, ML) and cortical surface (dorsoventral, DV): SNr (AP −5.5 mm, ML +2.2 mm, DV −7.7 mm); GPe (AP −0.96 mm, ML +2.8 mm, DV −5.8 mm). Following electrode implantation, the placement was sealed using dental acrylic and the wound site was further protected with surgical sutures. A post-surgical recovery period of at least 24 hours was given prior to fMRI acquisition for each subject.

2.3 Functional MRI

The DBS-fMRI experimental protocol is illustrated in Supplemental Figure S1. In preparation for fMRI procedures, rats were endotracheally intubated and mechanically ventilated using a small animal ventilator (CWE Inc., SAR-830/PA, Ardmore, PA). Anesthesia was initially maintained under constant isoflurane (1.5–2%) mixed with medical air. Tail vein catheterization was then performed for intravenous drug and contrast agent injections. Immediately following intubation and tail vein catheterization, animals were placed within a head-holder, and harnessed to a small animal cradle (both plastic and custom-made). The cradle was lined with a circulating water blanket connected to a temperature-adjustable water bath located outside the scanner room (Thermo Scientific, Waltham, MA). A rectal probe was used and core body temperature was maintained at 37 ± 0.5°C. Mechanical ventilation volume and rate were adjusted to maintain $EtCO_2$ of 2.8–3.2% and SpO_2 above 96%, using capnometry (Surgivet, Smith Medical, Waukesha, WI) and pulse oximetry (MouseOx Plus, STARR Life Science Corp., Oakmont, PA). $EtCO_2$ values from the capnometry system were previously calibrated against invasive sampling of arterial blood gas, reflecting a pCO_2 level of 30–40 mmHg (Shih et al., 2012; Shih et al., 2013).

MR images were acquired on a 9.4T Bruker BioSpec system with a BGA-9S gradient insert (Bruker Corp., Billerica, MA). A homemade single-loop surface coil with an internal

diameter of 1.6 cm, placed directly over the head, was used as a transceiver. Toothpaste was applied within the open coil loop to minimize MR susceptibility artifacts at the air-tissue interface. Magnetic field homogeneity was optimized first by global shim and followed by local first-order shims, and when necessary, local second-order shims using the FASTMAP protocol.

For anatomical referencing, a T_2-weighted RARE pilot image was taken in the mid-sagittal plane to localize the anterior commissure; this structure is located at approximately 0.8 mm posterior to the bregma and served as a reference for anteroposterior slice positioning in subsequent anatomical and functional scans. T_2-weighted anatomical images were obtained using a RARE sequence (scan parameters: TR = 2500 ms, TE = 33 ms, RARE factor = 8, slice thickness = 1 mm, matrix size= 256 × 256, FOV= 2.56 × 2.56 cm^2). Twelve axial slices were acquired, with the 5th slice from the anterior direction aligned with the anterior commissure (as acquired in the previous T_2-weighted pilot scan). The reduced electrode artifact, together with standardized slice positioning, rendered these images sufficient to localize the electrode tip placement, as previously described (Lai et al., 2015; Lai et al., 2014).

Following setup processes and immediately prior to CBV fMRI scan acquisition, rats were administered a monocrystalline iron oxide contrast agent (Feraheme; 30 mg Fe/kg, i.v.). Feraheme-based CBV measurements provide a well-established fMRI tool with a higher signal-to-noise ratio than traditional BOLD contrast imaging (Keilholz et al., 2006; Kim et al., 2013b; Silva et al., 2007; Wu et al., 2003; Zhao et al., 2009). Subsequently, anesthesia was switched to dexmedetomidine (dexdomitor; 0.05 mg/ml/hr, i.v.) cocktailed with the paralytic agent pancuronium bromide (0.5 mg/ml/hr, i.v.). This cocktail was administered for the remaining scan duration, continuously supplemented by 0.5% isoflurane (Fukuda et al., 2013).

CBV fMRI scans were acquired using a multi-slice single-shot gradient echo echo-planar imaging sequence (GE-EPI) (scan parameters: TR= 1000 ms, TE= 8.107 ms, slice thickness= 1 mm, matrix size= 80 × 80 (reconstructed to 128 × 128), FOV= 2.56 × 2.56 cm^2 and voxel size = 0.312 × 0.312 × 1 mm^3). Image slice geometry was imported from the previously acquired T_2-weighted anatomical image (12 slices).

2.4 Deep Brain Stimulation (DBS)

Simultaneous DBS with CBV fMRI was acquired in the same manner for all subjects, with bipolar and uniformly-distributed unilateral stimulation of the SNr or GPe. Each stimulation period consisted of a series of TTL-triggered biphasic, charge-balanced square-wave pulses with a pulse width of 500 μs and a stimulation intensity of 300 μA. A 90 second block design paradigm was implemented, consisting of a 20 second baseline period (stimulation OFF) followed by 10 seconds of stimulation ON, and an additional 60 seconds of rest (stimulation OFF). An additional rest period of at least two minutes was given between each DBS scan to allow for neurovascular recovery. Stimulation frequencies were varied in a pseudo-randomized order (10, 40, 70, 130, 200 and 400 Hz), and each DBS frequency scan was repeated 5-times per rat for within-subject/session averaging (see Section 2.5). The application of a fixed DBS pulse width, as used in this study, results in greater total charge

delivery with higher stimulation frequencies. However, this approach also removes the confounds associated with scaled pulse widths (used to control for charge density changes at varying stimulation frequencies), wherein different pulse widths may preferentially modulate varying neuronal elements (i.e., fibers and somata) (Kringelbach et al., 2007).

Immediately following evoked-fMRI scan acquisition, fcMRI scans were conducted in each subject. These scan series consisted of five, 5 minute scans during which either no stimulation or continuous DBS was applied (OFF and ON, respectively; ON consisted of stimulation of 300 μA, 500 μs pulse width, varied frequency). The fcMRI scans were conducted in succession without rest periods in the following order: $Rest_1$, Stim 40 Hz, $Rest_2$, Stim 130 Hz, and $Rest_3$.

2.5 Evoked-fMRI Data Processing and Statistical Analyses

Preprocessing and image analysis was performed using SPM codes and custom-written Matlab (MathWorks Inc., Natick, MA). Evoked-fMRI datasets were first grouped by subject and DBS frequency, and realigned to the first volume of a well-positioned subject using a least squares approach and a 6 parameter rigid body spatial transformation. Skull-stripping was next employed using a semi-automatic threshold method with manual masking, followed by image coregistration to an anatomical MRI rat atlas (Valdes-Hernandez et al., 2011). One SNr-DBS subject was excluded for evoked-fMRI analysis after image quality control.

Functional response maps for averaged SNr- or GPe-DBS datasets were generated using the general linear model (GLM), with reference to baseline (frames 1–20) and incorporating a hemodynamic delay of 5 frames, similar to our previous DBS-fMRI studies (Lai et al., 2015; Lai et al., 2014; Younce et al., 2014). A Bonferroni correction was applied to adjust for the multiple comparisons of fMRI maps by the number of brain voxels (corrected $p < 0.05$ for positive and negative responses). All images were smoothed by applying a mean filter with a 3 × 3 kernel, and overlaid on an anatomical atlas for visualization (Valdes-Hernandez et al., 2011).

For temporal analysis of DBS-evoked CBV changes, 3-dimensional regions of interest (ROIs) were defined *a priori* according to anatomical structural boundaries (Paxinos and Watson, 2004; Valdes-Hernandez et al., 2011), and applied onto the coregistered data. The ROIs were chosen according to the anatomical areas showing statistically significant modulation in the functional response maps. Nineteen ROIs were identified for analysis, all ipsilateral to the DBS target unless otherwise noted: cingulate cortex, dorsolateral striatum (ipsi- and contralateral), dorsomedial striatum (ipsi- and contralateral), GPe, infralimbic cortex, motor cortex, nucleus accumbens, orbitofrontal cortex, pedunculopontine tegmental nucleus, posterior hypothalamus, prelimbic cortex, SNr, somatosensory cortex, superior colliculus, ventral tegmental area, ventrolateral thalamus, and zona incerta (see Supplemental Figure S2). The baseline ΔR_2^* value was calculated as follows: Baseline $\Delta R_2^* = -1/TE \ln(S_{prestim}/S_0)$, where $S_{prestim}$ and S_0 represents MR signal intensity before each stimulation session (i.e., after Feraheme) and before Feraheme injection. Stimulus evoked ΔR_2^* values were calculated as follows: Stimulus evoked $\Delta R_2^* = -1/TE \ln(S_{stim}/S_{prestim})$, where S_{stim} and $S_{prestim}$ are the MR signal intensities during and before

stimulation, respectively. Cerebral blood volume changes were calculated by dividing stimulus-evoked ΔR_2* by baseline ΔR_2* values; because $S_{prestim}$ is used, this corrects for potential baseline drift and/or Feraheme washout. For each ROI, the CBV signal time-course was plotted across all 90 time frames.

DBS-evoked changes in CBV amplitude were also compared across stimulation frequencies and ROIs. Stimulus-evoked CBV responses were averaged across the stimulation period for each DBS frequency and ROI. These data are presented as mean ± SEM. Statistical comparisons of DBS frequency effects on ΔCBV for each ROI were conducted using Graphpad Prism software (San Diego, CA). Two-tailed, one-way repeated measures ANOVA (rANOVA) tests with Tukey post-hoc analyses were conducted to evaluate frequency-dependent responses. Significance level was set at $p < 0.05$.

2.6 fcMRI Data Processing and Statistical Analyses

Functional connectivity MRI datasets were preprocessed using the Analysis of Functional NeuroImages software suite (AFNI v2011-12-21-1014). The workflow included discarding the first 20 volumes, slice-timing correction, motion correction, alignment to a pre-existing high-resolution T_2-weighted template, spatial smoothing (Gaussian kernel FWHM = 1.5 mm), band-pass filtering (0.001 – 0.5 Hz), and regression of whole brain signal and the six motion parameters. The number of volumes discarded was increased from the traditional number (approximately 3–10) in order to ensure DBS-related changes from the initial stimulation were minimized. Furthermore, warping in the alignment procedure was limited to shifts and rotations to avoid unnecessary shearing and scaling of brain regions with signal drop-out associated with the DBS electrode. fcMRI analyses were conducted using the temporal correlation method. Fisher-Z transformed correlation matrices were generated using the average functional time series extracted for each region-of-interest (ROI) in the template atlas. Ipsilateral and contralateral hemispheres ROIs were analyzed separately yielding correlation matrices detailing mean within and between hemisphere connectivity (SNr: $n = 6$, GPe: $n = 7$). Individual connections were further evaluated across animals using repeated measures ANOVA models and categorized based on direction of effect. For each significant pairwise connection (rANOVA, $p < 0.01$) a basic correlation analysis was carried using a tent function and the resulting sign was used to categorize connections as either enhanced (increased correlation) or suppressed (increased anti-correlation). Each set of significantly modulated connections (enhanced or suppressed) was then reanalyzed using post-hoc ANOVAs in order to test the overall effect of condition: $Rest_{1\text{-}3}$, 40 Hz, and 130 Hz. Pair-wise connections with weak modulation ($|\Delta Z\text{-corr.}| < 0.10$) were ignored. Significant main-effects were followed by pair-wise comparisons to test for significant differences between conditions. Furthermore, in order to assess the potential contribution of global signal regression (GSR), these analyses were repeated using data without GSR. The global signal across conditions and animals was also compared. Specifically, we calculated the pairwise Fisher's Z-correlation of the global signal across stimulation conditions ($Rest_{1\text{-}3}$, 40 Hz, and 130 Hz) and animals resulting in 10 pairs per animal. These values were then analyzed using repeated measures ANOVA to determine if there was an overall effect, i.e. a difference in the temporal correlation, which would suggest that one or more of the

global signals vary as a function of condition. Finally, connections were grouped based on network classifications (sensorimotor, executive, limbic, and between network connections).

3 Results

The setup for the surface coil and implanted tungsten microwire is shown in Figure 1A. Electrode tip placements within the SNr and GPe were verified for each subject using T_2-weighted RARE anatomical images using methods described previously (Lai et al., 2015; Lai et al., 2014; Younce et al., 2014) (Figure 1B–C). Animals with electrode placements outside of the target regions were discarded from the study and excluded from all further experimental analyses. They were not included in the final subject numbers.

3.1 Evoked fMRI

Both SNr- and GPe-DBS produced significant and frequency-dependent CBV responses in several brain structures both within and outside the basal ganglia (Functional response maps: Figure 2: 40 and 130 Hz; Supplemental Figures S4–5: all other frequencies; Supplemental Figure S3: 130 Hz SNr-DBS displayed on EPI). In addition to generating functional response maps, CBV time-courses for each DBS target and stimulation frequency were calculated for 19 anatomical ROIs (Figures 3–4 **and** Supplemental Figures S6–7; see also Supplemental Figure S8 for a representative example of non-averaged CBV timecourses, demonstrating reproducibility of evoked fMRI responses across trials).

10 Hz DBS at either target produced no significantly modulated voxels, including within the electrode target region (see Supplemental Figures S4 and S5). In contrast, significant and extensive CBV modulation was noted at all other frequencies tested (40–400 Hz). The spatial pattern of CBV modulation was qualitatively similar across stimulation frequencies, and in some respects also similar between SNr and GPe stimulation targets. For example, both GPe- and SNr-DBS resulted in CBV changes predominantly ipsilateral to the stimulation site, with the exception of the dorsal striatum, which was bilaterally modulated by DBS at either target. SNr-DBS produced negative CBV changes bilaterally in striatum, whereas GPe-DBS produced a pattern of positive and negative CBV changes in the ipsi- and contralateral dorsal striatum, respectively. Also of note, a “double peak” of CBV modulation was a characteristic response to DBS in certain regions, including the ipsilateral somatosensory cortex (both DBS targets), and dorsal striatum (SNr-DBS) (Figures 3–4), possibly due to the recruitment of two distinct circuitries or a delayed neurotransmission effect. Future work is necessary to confirm the neuronal mechanism(s) underlying this double-peak response.

SNr-DBS (40–400 Hz) evoked positive CBV changes in multiple basal ganglia nuclei (GPe, substantia nigra), as well as additional areas intimately tied to the basal ganglia (pedunculopontine tegmental nucleus, zona incerta, ventral tegmental area) (see Figure 3 and Supplemental Figure S6). Of all regions examined, the substantia nigra showed the largest CBV changes (nearly 30% CBV increases at 200 or 400 Hz DBS). In stark contrast to GPe-DBS, frontal and prefrontal cortical modulation by SNr-DBS was relatively sparse; functional activation maps revealed spatially restricted vasodilation (e.g., in cingulate cortex), as well as contralateral vasoconstriction in prefrontal cortex (most apparent at 130

Hz). However, a closer examination of this data by means of CBV traces revealed that many of these areas (e.g., motor, somatosensory, prelimbic cortices) were likely positively modulated by 200 Hz SNr-DBS, albeit with a long delay (and thus not detected with our functional activation maps). Also of note, the superior colliculus, which receives direct innervation from the SNr (Deniau et al., 2007; Kaneda et al., 2008), had little to no detectable CBV changes during SNr-DBS.

During GPe-DBS (40–400 Hz), robust CBV increases were observed in ipsilateral frontal and prefrontal cortices, including cingulate, motor, prelimbic, infralimbic, and orbitofrontal cortices. A wealth of subcortical areas also showed positive CBV responses, including the substantia nigra, nucleus accumbens, ventral tegmental area, zona incerta, and others (see Figure 4 and Supplemental Figure S7). Of all regions examined, peak CBV responses to GPe-DBS were strongest in orbitofrontal cortex, reaching nearly 30% CBV increases with 400 Hz stimulation.

Lastly, to determine the frequency-dependency of DBS responses at both targets, the amplitude of CBV responses was quantified for a subset of ROIs: GPe, substantia nigra, dorsolateral striatum (ipsi- and contralateral, somatosensory cortex, posterior hypothalamus (SNr-DBS only), and prelimbic cortex (GPe-DBS only) (Figure 3–4). These amplitude measures correspond to the mean CBV changes during the stimulation epoch for each DBS frequency (see Methods); because of differences in the characteristic trace dynamics for each ROI (e.g., hemodynamic delays), the calculated values are best compared across frequencies but not across ROI's. A main effect of DBS frequency was found for each ROI analyzed ($p < 0.05$), and post-hoc testing revealed that 10 Hz DBS drove CBV amplitude changes that often significantly differed from other frequencies. However, as suggested by the CBV traces, the influence of stimulation frequency on CBV responses was inconsistent across ROIs. For example, CBV amplitudes for some ROIs scaled positively with DBS frequency (e.g., the GPe during SNr-DBS), whereas peak amplitudes occurred at frequencies below 400 Hz for other ROIs (e.g., prelimbic and somatosensory cortices during SNr-DBS) (see Figures 3 **and** S6).

3.2 fcMRI

Complementing our evoked-fMRI findings, fcMRI measurements revealed global and frequency-dependent modulation by DBS at both targets. Mean correlation matrices were generated for each stimulus condition ($Rest_1$, Stim 40 Hz, $Rest_2$, Stim 130 Hz, and $Rest_3$) and DBS target (SNr and GPe); Figure 5A. The cross-correlational matrices, displaying functional connectivity strength between 90 discrete brain regions (45 per hemisphere), revealed modulation that appeared specific to the 130 Hz DBS condition, including both enhancements (increased correlation) and suppressions (increased anti-correlation) of connectivity. This modulation of fcMRI signals appeared moderately reversible, as the post 130 Hz stimulation "rest" scan (conducted immediately following the 130 Hz DBS fcMRI scan), was qualitatively similar to prior non-stimulation scans. Functional connectivity modulation by 40 Hz DBS was less apparent at both targets. Significant individual fcMRI connections were computed (rANOVA, $p < 0.01$ uncorrected, $\Delta Z\text{-Corr} > 0.10$) and categorized according to modulation direction; Supplemental Tables S1 (SNr) and Table S2

(GPe). Post-hoc comparison of the significantly modulated connections confirmed the qualitative observations; Figure 5B. For both DBS targets (SNr and GPe) and modulation directions (Enhanced and Suppressed) there was a significant main-effect of condition (ANOVA $p < 0.001$); SNr: $F_E(4,165) = 25.13$ and $F_S(4,75) = 11.79$; GPe: $F_E(4,190) = 24.39$ and $F_S(4,190) = 26.49$. Further post-hoc pair-wise comparisons between conditions revealed 130 Hz stimulation specificity; i.e. 130 Hz was significantly different from all rest conditions and 40 Hz stimulation, $p < 0.001$. Furthermore, no statistical differences were detected between any other conditions, including $Rest_3$, suggesting the stimulation effect was indeed reversible. Several connections showed more robust modulation (Figure 6, and see Supplemental Tables S1–2: $|\Delta Z\text{-Corr}| > 0.20$). Here, we focus on describing the enhanced connections given the potential confound of global signal regression (see next paragraph). Specifically, SNr-DBS produced several ipsilateral enhancements: VTA (#15) ↔ Insula (#5), pHyp (#28) ↔ Insula (#5), STN (#31) ↔ GPe (#21), ZI (#39) ↔ GPe (#21), ZI (#39) ↔ GPe (#STN). Only one connection demonstrated robust enhancement in the contralateral hemisphere: SNr-DBS, dHipp (#85) ↔ Somato (#77). Similarly, GPe-DBS produced robust ipsilateral enhancement for the following connections; Motor (#22) ↔ Insula (#5), ZI (#39) ↔ Insula (#5), VC (#38) ↔ AC (#16), and ZI (#39) ↔ Motor (#22).

In order to assess the sensitivity of the observed enhancements/suppressions to GSR, we recapitulated the post-hoc comparisons of the previously defined modulated connections using pre-processed data without GSR. The main-effect of condition for both DBS targets was maintained for enhanced but not for suppressed connections (**see** Supplemental Figure S9); SNr: $F_E(4,165) = 6.81$, $p < 0.001$ and $F_S(4,75) = 0.92$, $p = 0.460$; GPe: $F_E(4,190) = 5.71$, $p < 0.001$ and $F_S(4,190) = 1.85$, $p = 0.121$. Some trends were still evident for the suppressed connections however all conditions and groupings exhibited substantial shifts towards more positive values. Moreover, 130 Hz specificities were maintained for the enhanced connections; SNr $p \leq 0.016$, GPe ≤ 0.006. Finally, we further evaluated the similarity (cross-correlation) of the global signal (GS) across conditions. The main-effect of condition was insignificant for both DBS targets suggesting there was a high degree of similarity in the GS regardless of condition (rANOVA); SNr: $F(9,45) = 1.63$, $p = 0.134$; GPe: $F(9,54) = 0.85$, $p = 0.572$.

Next, significant modulations were considered in the context of functional network groupings: Sensorimotor, Executive, Limbic, and Between network connections. Categorical listing for each brain region are provided in the supporting material; Supplemental Tables S1–2. Between network connections reflect connections that crossed functional category (e.g., between sensorimotor and limbic regions). Of connections meeting significance criteria, a larger proportion of enhancements were observed for the SNr: 34 enhanced, 16 suppressed. Enhancement and suppression were equivalent for GPe stimulation; 39 enhanced and suppressed. In terms of overall network modulation, most DBS-sensitive connections fell within the Between network category (SNr: 33; GPe, 48) followed by the Sensorimotor, Limbic, Executive networks, respectively. Finally, many of the robust modulations either localized to the Sensorimotor network, or involved sensorimotor regions.

4 Discussion

The present study was undertaken to map the functional circuit and network connectivity of the SNr and GPe, using an unbiased DBS-fMRI approach. This work was motivated by a number of recent studies demonstrating unanticipated anatomical and functional connectivity among these regions (reviewed in Introduction), which have diverse roles in motor control, cognition, and emotional processing. We employed a large range of target stimulation frequencies to identify circuit and network connections that may be selectively modulated at specific frequency ranges, both to better understand inherent circuit/network properties, as well as for the relevance of such comparisons for therapeutic DBS applied at these targets. Broadly, although both the SNr and GPe have traditionally been classified as simple relay nuclei, our DBS results reveal extensive functional circuit and network interconnectivity, consistent with substantial “extra-relay” processing power. Below, we highlight the major findings and limitations of this work.

4.1 Frequency-dependency of evoked DBS responses

The usage of multiple stimulation frequencies in DBS-fMRI studies allows for the characterization of frequency tuning in neural circuits (Canals et al., 2008; Krautwald and Angenstein, 2012; Lai et al., 2015; Lai et al., 2014; Paek et al., 2015; Shih et al., 2014b). The demonstration of DBS frequency-sensitive fMRI signals Is likely due to both passive and active electrical membrane properties, including voltage-sensitive ion channel complements and their associated channel refractory periods (Kringelbach et al., 2007). 10 Hz stimulation of either the SNr or GPe did not result in any detectable fMRI signal changes (likely reflecting neuronal activity changes subthreshold for fMRI signal detection in our setup), while the stimulation frequency that evoked the largest CBV responses varied considerably by region. Perhaps the most compelling example of frequency selective circuit modulation in the present study occurred with 200 Hz SNr-DBS. At both lower and higher frequencies (40–130, 400 Hz), prefrontal and frontal cortical regions (e.g., infralimbic, motor, cingulate cortices) responded to SNr-DBS with CBV increases that were modest and time-locked to the stimulation period. However, these brain regions responded to 200 Hz stimulation with CBV increases that were much larger than at other frequencies, and peaked with a long delay (in certain case, after the cessation of stimulation). The reasoning behind such remarkably frequency selectivity in these responses, with highly unique temporal characteristics (in relation to the stimulation period), is an interesting area for future study. Finally, the inclusion of very high stimulation frequencies in the present study (e.g., 130 Hz) is notable in the context of therapeutic DBS (see Section 4.5).

4.2 Striatal and Thalamic CBV modulation by SNr- and GPe-DBS

Both the GPe- and SNr are downstream targets of the striatum, receiving GABAergic input through the so-called indirect and direct pathways, respectively. Although striatal activity changes may thus be anticipated during either GPe- or SNr-DBS, our demonstration of striatal modulation by DBS at each target is of remarkable interest for several reasons. First, although the basal ganglia are frequently modeled as intrahemispheric systems, we observed pronounced bilaterality in striatal modulation by GPe- or SNr-DBS. Irrespective of whether this modulation occurs through feedforward thalamo-cortico-striatal loops, antidromic

recruitment of striatal fibers, or other means, our results contribute to a growing body of literature demonstrating bilateral functional connectivity within the basal ganglia system (Brun et al., 2012; Fox et al., 2016; Liu and Basso, 2008; Min et al., 2012; Novak et al., 2009). Of further interest is the directionality of this striatal hemodynamic response; prominent CBV decreases were noted within the dorsal striatum during DBS of either the SNr or GPe, and occurred across a wide range of stimulation frequencies (40 Hz and higher). Such striatal vasoconstriction is highly reminiscent of fMRI responses obtained during evoked nociceptive peripheral stimulation (Shih et al., 2009; Zhao et al., 2008). The extent and magnitude of the DBS-evoked signals was greater at the SNr target compared to the GPe, and was also greater in the hemisphere contralateral to stimulation (although ipsilateral decreases were also observed with both DBS targets). Although it may be intuitive to interpret our data as DBS-evoked neuronal inhibition, the situation appears to be particularly muddled in striatum, wherein dopaminergic neurotransmission has been hypothesized to induce vasoconstriction independent of direct activity changes within striatal neurons (Hsu et al., 2014) or regional metabolism (Shih et al., 2011). In addition, striatal CBV decreases have previously been shown with heightened local neuronal activity, as observed in rats during noxious forepaw stimulation (Shih et al., 2009; Shih et al., 2014a), or epileptic slow-wave discharge (Mishra et al., 2011). In light of these complexities, further work will be necessary to determine the underlying mechanism of striatal CBV decreases evoked during GPe- and SNr-DBS.

The directionality of CBV responses was also perplexing in the basal ganglia output-receiving thalamic areas (e.g., ventral thalamus), which are modeled as receiving functionally antagonistic modulation by the GPe and SNr (Albin et al., 1989; DeLong, 1990). The framework of this model, and the observation that electrical stimulation of the rat SNr generates GABA-mediated inhibition in ventral thalamus (MacLeod et al., 1980), suggest that SNr-DBS should drive CBV signal decreases in ventral thalamus (and other nigral outputs) consistent with neuronal inhibition. Yet, we observed only positive CBV responses in thalamic regions during DBS delivered at either the GPe or SNr. Among the many possible explanations for SNr-DBS evoked thalamic CBV increases are: 1) bona fide thalamic activity increases downstream of non-canonical nigral circuits; 2) “off target” circuit modulation due to the nonselectivity of electrical stimulation (discussed in Section 4.6, Limitations); and 3) neurovascular uncoupling mechanisms similar to as discussed for the striatal CBV signals. Future DBS-fMRI studies coupled with more selective stimulation modalities (e.g., optogenetics) and electrophysiological recordings will be necessary to distinguish between these possibilities.

4.3 Frontal cortical CBV increases evoked by GPe-DBS

One major unexpected finding in this study was the robust modulation of frontal cortical areas (including prefrontal and motor cortices) by GPe-DBS. Historically, the GPe has been viewed primarily as a basal ganglia relay nucleus with only indirect control over cortical activity (Albin et al., 1989; DeLong, 1990). Very recently, however, two studies have identified a direct, ipsilateral projection from GPe to frontal cortex in mouse, rat, and monkey (Chen et al., 2015; Saunders et al., 2015). The GPe neurons that make up this projection are GABAergic and express the GABA vesicular transporter (vGAT), with a large

subset additionally being cholinergic (expressing choline acetyltransferase (ChAT)). This pathway innervates all layers of cortex, targeting both pyramidal cells and interneurons. Unsurprisingly, selective optogenetic stimulation of this pathway results in mixed patterns of modulation among frontal cortical neurons, with both inhibition and enhanced firing rates observed *in vivo* (Saunders et al., 2015). As expected based on neurochemical makeup, selective stimulation of this projection is predominantly inhibitory for cortical neurons. However, given that this projection has been reported to biasedly innervate cortical interneurons, it is possible that distant inhibitory mechanisms result in enhanced cortical activity and vasodilatation. The robust modulation of frontal cortex by GPe-DBS observed in the present study may be the result of such pallido-cortical transmission, although the use of nonselective electrical stimulation precludes a definitive interpretation.

4.4 fcMRI

Complementing our evoked-fMRI findings, fcMRI measurements revealed frequency-dependent functional connectivity modulation by DBS at both targets. More specifically, we observed significant modulation of global functional connectivity (compared to baseline scans) with 130 Hz, but not 40 Hz, stimulation. This observed frequency-dependence of DBS-induced fcMRI network modulation is perplexing in that robust circuit modulation (measured with evoked-fMRI) was observed at both 40 and 130 Hz DBS. It is not clear why 40 Hz DBS of the GPe or SNr was insufficient to significantly modulate fcMRI networks, however this finding suggests that fcMRI networks may be more rigid than evoked-fMRI circuits (although this interpretation is highly speculative). The GPe and SNr are both pacemaker nuclei, with some neurons exhibiting intrinsic firing rates as high as 50 Hz (GPe) and 80 Hz (SNr) (Abdi et al., 2015; Deniau et al., 2007). It is possible that, given these relatively high intrinsic firing rates, exogenous stimulation by DBS may need to be employed at very high frequencies (e.g., 130 Hz) to override the normal network contributions of the GPe and SNr.

During GPe- and SNr-DBS at 130 Hz, both enhancements and suppressions in functional connectivity were noted between a wide number of brain regions, spanning large-scale functional and anatomical boundaries. Interestingly, compared to enhanced connections, suppressed (i.e. shifts towards negative connectivity) demonstrated much greater sensitivity to global signal regression. Increased sensitivity to “negative correlations” following GSR has been well documented in BOLD fcMRI studies (Yan et al., 2013), therefore GSR may have similar effects on CBV-based connectivity. CBV-weighted functional connectivity has been shown to largely mirror BOLD-based connectivity in the rat (Magnuson et al., 2010), though with lower overall connectivity strength and slightly different frequency spectra. Overall, functional connectivity studies using cerebral blood measures are still relatively scarce, and thus interpretations should be made with caution. This is particularly the case given that GSR remains a controversial topic in the BOLD fcMRI field (Murphy et al., 2009; Yan et al., 2013), therefore we are hesitant to draw any major conclusions from the observed “suppression” effects. Nonetheless, it is important to note that suppressed connections were only detected after accounting for large-scale CBV-weighted changes.

Focusing on enhanced connections, the most robust effects were largely ipsilateral to the DBS target and demonstrated interesting patterns. Some spatial overlap between enhanced networks was observed, with the insula and zona incerta appearing in both DBS-targeted networks (Figure 6). Consistent with the evoked responses, SNr-DBS enhanced connectivity involving the GPe and dorsal striatum (Table S1), however connectivity with the latter was not enhanced by GPe-DBS. This could be related to the fact that mixed (positive and negative) evoked responses were observed in the ipsilateral striatum during GPe-DBS, suggesting that more specific ROIs might be necessary to detect related functional connectivity modulation. Also of note, most enhanced connections did not directly involve the DBS target, but rather downstream and/or polysynaptic targets, particularly 'between' networks (Sensorimotor, Executive, and Limbic). The ability to manipulate functional circuits using exogenous sources, as demonstrated here, has the potential to elucidate unique relationships between evoked signals and functional connectivity changes, and their relationships in different disease models; however, further experimentation/considerations are necessary, particularly in the context of GSR as outlined above. To our knowledge, this work provides the first example of electrical DBS-induced frequency-dependent functional connectivity modulation.

4.5 Translational Relevance

High frequency DBS targeting select brain nuclei or fiber tracts is now routinely employed in clinical settings for the treatment of certain intractable neurological and neuropsychiatric disorders (Goodman and Alterman, 2012; Lozano and Lipsman, 2013). The most prominent examples of successful DBS therapy are perhaps the targeting of the subthalamic nucleus (STN) or internal globus pallidus (GPi) for motor symptom alleviation in late-stage Parkinson's disease (Moro et al., 2010; Okun, 2012). Given the dense interconnectivity of the basal ganglia, and the ability of DBS to modulate large-scale circuits and networks (Wichmann and Delong, 2011), it is not surprising that other basal ganglia nuclei have emerged as promising targets for DBS therapy (at least for those diseases involving basal ganglia dysfunction). Indeed, both SNr- and GPe-DBS have been reported to alleviate motor signs in Parkinson's disease, with unique therapeutic profiles compared to STN/GPi-DBS (Chastan et al., 2009; Vitek et al., 2004; Weiss et al., 2013). For example, in a small group of advanced Parkinson's patients with bilateral DBS lead implants targeted for the STN, but also reaching the SNr, it was reported that DBS isolated to the SNr-residing contacts selectively alleviated axial, but not distal motor symptoms (STN-DBS reduced both categories of symptoms) (Chastan et al., 2009). This result encourages further examination of SNr-DBS for the treatment of patients in which postural and balance deficits predominate (Fasano et al., 2015). In this context, it is interesting to note that, in decerebrate cats, acute electrical stimulation of the pedunculopontine tegmental nucleus (PPTg) induced loss of postural tone that was rescued via conditioning electrical stimulation of the SNr (Takakusaki et al., 2004). Thus, downstream modulation of the PPTg, also identified in our setup during SNr- (and GPe)-DBS (see Supplemental Figures S6–7), is an attractive candidate mechanism for DBS-induced alleviation of postural deficits. Similar to the case for the SNr target, GPe-DBS has yet to be extensively investigated for Parkinson's disease treatment, although an exploratory study of high frequency GPe stimulation in patients undergoing a pallidotomy procedure has confirmed DBS-induced motor symptom relief, including

reductions in bradykinesia (Vitek et al., 2004). There is also emerging evidence that SNr-DBS and/or GPe-DBS may be clinically useful beyond the treatment of Parkinson's disease; for example, recent animal and patient studies of SNr-DBS have shown promise for the treatment of epilepsy (Guo et al., 2014; Shi et al., 2006; Velisek et al., 2002; Wille et al., 2011), whereas at least one case study has reported Tourette's syndrome symptom reductions during GPe-DBS (Piedimonte et al., 2013).

Several findings in the present study may aid in the understanding of the neural mechanisms of GPe- and SNr-DBS therapy. Although GPe- and SNr-DBS have not been rigorously compared in the clinical setting, our findings suggest that both overlapping and distinct neural circuits may be modulated by these therapies. Among the most notable distinctions, ipsilateral prefrontal and frontal cortical areas were modulated to a far greater degree (as measured by evoked-fMRI) with GPe- compared to SNr-DBS. Given such profound differences in DBS-evoked circuit modulation, distinct therapeutic and/or adverse clinical responses would not be unexpected between DBS applied at each target. Also of interest is the presence of bilateral striatal responses during DBS at both targets. Therapeutic DBS, even applied unilaterally, can often exert bilateral behavioral responses (Okun, 2012), although the neural mechanisms underlying such response bilaterality are poorly understood. Our findings identify the contralateral striatal modulation as a candidate mechanism underlying bilateral clinical responses during both GPe- and SNr-DBS.

4.6 Limitations

Our study includes several limitations that are generally characteristic of preclinical fMRI-DBS experiments. The usage of anesthesia, as is commonly employed in preclinical fMRI experiments (Haensel et al., 2015; Krautwald and Angenstein, 2012; Lai et al., 2014; Min et al., 2012), may alter the responsivity of neural circuits to the effects of DBS. One possible means by which an anesthetic effect may be evident could be in the stimulation strength threshold for detectable fMRI responses. Although not systematically tested at the SNr and GPe stimulation targets, in pilot experiments in which DBS was applied to the nucleus accumbens (but otherwise under similar experimental conditions to the present study), we were unable to reliably achieve evoked or functional connectivity fMRI responses with current amplitudes below 300 μA (Albaugh et al., 2016). Thus, our DBS-fMRI experiments have generally relied upon higher amplitudes than those generally used in preclinical DBS studies in awake rodents (typically 100–150 μA) (Ewig et al., 2013; Hamani et al., 2014; Vassoler et al., 2008), although higher amplitudes have been reported for studies in both awake and anesthetized states (McCracken et al., 2007; van Dijk et al., 2013). We also note that the employed pulse duration of 500 μs is higher than that traditionally used in clinical DBS (in the approximate range of 60–100 μs), although longer pulse durations are not uncommon in DBS-fMRI animal studies under anesthetized conditions (Kim et al., 2013a; Min et al., 2012). We postulate that relatively higher current amplitudes (i.e. 300 μA) may have been necessitated by the usage of anesthesia in our model or the sensitivity of our fMRI procedure. This in turn increases the possibility of "off-target" stimulation effects, due to current spread outside the anatomical boundaries of the target regions. Future studies may rely upon conscious animal imaging to tackle these potential limitations (Ferenczi et al., 2016; Ferris et al., 2006).

With respect to our fcMRI experiments, DBS was employed continuously for 5 min durations- a stimulation length that has the potential to introduce drastic physiological changes. However, in our experiments, network responses to DBS appeared largely reversible, as the post-DBS period connectivity was qualitatively and quantitatively similar to pre-DBS. The network-level responses to continuous DBS are also interesting to study in the context of clinical DBS therapy, wherein continuously-applied stimulation may be used to correct pathological network activity (Okun, 2012; Wichmann and Delong, 2011). Nonetheless, it may be beneficial in future DBS-fMRI studies to explore the use of interleaved DBS OFF-ON-OFF fcMRI paradigms with shorter stimulation periods.

The use of electrical stimulation for circuit mapping may be viewed as either a strength or weakness in the present study; it is highly translationally-relevant in the context of clinical DBS therapy, yet comes with limitations of circuit recruitment specificity. As suggested above, electrical stimulation may be prone to off-target circuit recruitment, and may present another limitation to the present study. Electrical stimulation is capable of recruiting fibers of passage, and current may also spread beyond the anatomical boundaries of the target region; in either instance, “off-target” areas may be recruited by DBS. An additional, related point concerns the directionality of connectivity between the DBS target region and other modulated areas. Because DBS can recruit connected brain areas through both ortho- and antidromic signal propagation across fibers (Grill et al, 2008; Li et al., 2012) this approach to functional circuit mapping cannot readily distinguish between up- and downstream circuit elements. The use of opto- and/or pharmacogenetic tools should provide a more precise means for functional imaging-based circuit mapping (Ferenczi et al., 2016; Lee et al., 2010; Michaelides et al., 2013), although at the likely expense of translational relevance in the context of therapeutic DBS in clinical settings.

5 Conclusions

This study implemented a simultaneous DBS-fMRI approach to investigate the functional connectivity of the GPe and SNr, the two major striatal output nuclei. Through their roles in the basal ganglia loops, these regions have a diverse number of functional roles in cognition, motor control, and emotional processing. As demonstrated here and elsewhere, DBS-fMRI provides a global perspective of a brain region’s functional connectivity profile, ultimately allowing for the identification and characterization of novel circuit connections. In the present work we identified, among other results, DBS-evoked negative fMRI signals in the bilateral striatum, as well as frequency-dependent, large-scale functional connectivity changes. Broadly, our work contributes to a growing literature demonstrating functional connectivity of the striatal outputs outside of canonical thalamic relay connections. Further, the inclusion of high frequency stimulation in our DBS experiments facilitates a translational perspective on our connectivity maps, as high frequency DBS at the GPe or SNr has demonstrated therapeutic benefits in certain neurological disease states (e.g., Parkinson’s Disease).

Supplementary Material

Refer to Web version on PubMed Central for supplementary material.

Acknowledgments

Grant support

D.L.A. was supported by the National Institute of Neurological Disorders and Stroke (NINDS) (NS087909). N.V.D.B. was supported by the Research Foundation Flanders. G.D.S. was supported by the Klarman Family Foundation, the Brain and Behavior Research Foundation, the Foundation for Prader-Willi Research, the Foundation of Hope, the National Institute on Drug Abuse (DA032750 and DA038168), and the Department of Psychiatry at UNC Chapel Hill. W.G. was supported by the NINDS (NS088975) and Cedars-Sinai Medical Center. Y.Y.I.S. was supported by the NINDS (NS091236), the National Institute of Mental Health (MH106939), the National Institute on Alcohol Abuse and Alcoholism (AA020023), the National Institute of Health UL1TR001111 sub-awards 550KR81420 and 550KR91413, the Brain and Behavior Foundation Young Investigator Award and Ellen Schapiro & Gerald Axelbaum Investigator fund, the American Heart Association Scientist Development Award (15SDG23260025), and the Department of Neurology and the Biomedical Research Imaging Center at UNC Chapel Hill.

References

Abdi A, Mallet N, Mohamed FY, Sharott A, Dodson PD, Nakamura KC, Suri S, Avery SV, Larvin JT, Garas FN, Garas SN, Vinciati F, Morin S, Bezard E, Baufreton J, Magill PJ. Prototypic and arkypallidal neurons in the dopamine-intact external globus pallidus. J Neurosci. 2015; 35:6667–6688. [PubMed: 25926446]

Albaugh DL, Salzwedel A, Van Den Berge N, Gao W, Stuber GD, Shih YY. Functional Magnetic Resonance Imaging of Electrical and Optogenetic Deep Brain Stimulation at the Rat Nucleus Accumbens. Sci Rep. 2016; 6:31613. [PubMed: 27601003]

Albaugh DL, Shih YY. Neural circuit modulation during deep brain stimulation at the subthalamic nucleus for Parkinson's disease: what have we learned from neuroimaging studies? Brain Connect. 2014; 4:1–14. [PubMed: 24147633]

Albin RL, Young AB, Penney JB. The functional anatomy of basal ganglia disorders. Trends Neurosci. 1989; 12:366–375. [PubMed: 2479133]

Brun Y, Karachi C, Fernandez-Vidal S, Jodoin N, Grabli D, Bardinet E, Mallet L, Agid Y, Yelnik J, Welter ML. Does unilateral basal ganglia activity functionally influence the contralateral side? What we can learn from STN stimulation in patients with Parkinson's disease. J Neurophysiol. 2012; 108:1575–1583. [PubMed: 22745463]

Calabresi P, Picconi B, Tozzi A, Ghiglieri V, Di Filippo M. Direct and indirect pathways of basal ganglia: a critical reappraisal. Nat Neurosci. 2014; 17:1022–1030. [PubMed: 25065439]

Canals S, Beyerlein M, Merkle H, Logothetis NK. Functional MRI evidence for LTP-induced neural network reorganization. Curr Biol. 2009; 19:398–403. [PubMed: 19230667]

Canals S, Beyerlein M, Murayama Y, Logothetis NK. Electric stimulation fMRI of the perforant pathway to the rat hippocampus. Magn Reson Imaging. 2008; 26:978–986. [PubMed: 18479870]

Chastan N, Westby GW, Yelnik J, Bardinet E, Do MC, Agid Y, Welter ML. Effects of nigral stimulation on locomotion and postural stability in patients with Parkinson's disease. Brain. 2009; 132:172–184. [PubMed: 19001482]

Chen MC, Ferrari L, Sacchet MD, Foland-Ross LC, Qiu MH, Gotlib IH, Fuller PM, Arrigoni E, Lu J. Identification of a direct GABAergic pallidocortical pathway in rodents. Eur J Neurosci. 2015; 41:748–759. [PubMed: 25581560]

Cui G, Jun SB, Jin X, Pham MD, Vogel SS, Lovinger DM, Costa RM. Concurrent activation of striatal direct and indirect pathways during action initiation. Nature. 2013; 494:238–242. [PubMed: 23354054]

DeLong MR. Primate models of movement disorders of basal ganglia origin. Trends Neurosci. 1990; 13:281–285. [PubMed: 1695404]

Deniau JM, Mailly P, Maurice N, Charpier S. The pars reticulata of the substantia nigra: a window to basal ganglia output. Prog Brain Res. 2007; 160:151–172. [PubMed: 17499113]

Dunn JF, Tuor UI, Kmech J, Young NA, Henderson AK, Jackson JC, Valentine PA, Teskey GC. Functional brain mapping at 9.4T using a new MRI-compatible electrode chronically implanted in rats. Magn Reson Med. 2009; 61:222–228. [PubMed: 19097225]

Fasano A, Aquino CC, Krauss JK, Honey CR, Bloem BR. Axial disability and deep brain stimulation in patients with Parkinson disease. Nat Rev Neurol. 2015; 11:98–110. [PubMed: 25582445]

Ferenczi EA, Zalocusky KA, Liston C, Grosenick L, Warden MR, Amatya D, Katovich K, Mehta H, Patenaude B, Ramakrishnan C, Kalanithi P, Etkin A, Knutson B, Glover GH, Deisseroth K. Prefrontal cortical regulation of brainwide circuit dynamics and reward-related behavior. Science. 2016; 351:aac9698. [PubMed: 26722001]

Ferris CF, Febo M, Luo F, Schmidt K, Brevard M, Harder JA, Kulkarni P, Messenger T, King JA. Functional magnetic resonance imaging in conscious animals: a new tool in behavioural neuroscience research. J Neuroendocrinol. 2006; 18:307–318. [PubMed: 16629829]

Fox ME, Mikhailova MA, Bass CE, Takmakov P, Gainetdinov RR, Budygin EA, Wightman RM. Cross-hemispheric dopamine projections have functional significance. Proc Natl Acad Sci U S A. 2016; 113:6985–6990. [PubMed: 27298371]

Freeze BS, Kravitz AV, Hammack N, Berke JD, Kreitzer AC. Control of Basal Ganglia output by direct and indirect pathway projection neurons. J Neurosci. 2013; 33:18531–18539. [PubMed: 24259575]

Friend DM, Kravitz AV. Working together: basal ganglia pathways in action selection. Trends Neurosci. 2014; 37:301–303. [PubMed: 24816402]

Fukuda M, Vazquez AL, Zong X, Kim SG. Effects of the alpha(2)-adrenergic receptor agonist dexmedetomidine on neural, vascular and BOLD fMRI responses in the somatosensory cortex. Eur J Neurosci. 2013; 37:80–95. [PubMed: 23106361]

Gittis AH, Berke JD, Bevan MD, Chan CS, Mallet N, Morrow MM, Schmidt R. New roles for the external globus pallidus in basal ganglia circuits and behavior. J Neurosci. 2014; 34:15178–15183. [PubMed: 25392486]

Goldberg JH, Farries MA, Fee MS. Basal ganglia output to the thalamus: still a paradox. Trends Neurosci. 2013; 36:695–705. [PubMed: 24188636]

Goodman WK, Alterman RL. Deep brain stimulation for intractable psychiatric disorders. Annu Rev Med. 2012; 63:511–524. [PubMed: 22034866]

Guo H, Zhang H, Kuang Y, Wang C, Jing X, Gu J, Gao G. Electrical stimulation of the substantia nigra pars reticulata (SNr) suppresses chemically induced neocortical seizures in rats. J Mol Neurosci. 2014; 53:546–552. [PubMed: 24399411]

Haensel JX, Spain A, Martin C. A systematic review of physiological methods in rodent pharmacological MRI studies. Psychopharmacology (Berl). 2015; 232:489–499. [PubMed: 25585682]

Hsu YH, Chang C, Chen CC. Negative cerebral blood volume fMRI response coupled with Ca(2)(+)-dependent brain activity in a dopaminergic road map of nociception. Neuroimage. 2014; 90:43–51. [PubMed: 24369291]

Jahfari S, Waldorp L, van den Wildenberg WP, Scholte HS, Ridderinkhof KR, Forstmann BU. Effective connectivity reveals important roles for both the hyperdirect (fronto-subthalamic) and the indirect (fronto-striatal-pallidal) fronto-basal ganglia pathways during response inhibition. J Neurosci. 2011; 31:6891–6899. [PubMed: 21543619]

Kaneda K, Isa K, Yanagawa Y, Isa T. Nigral inhibition of GABAergic neurons in mouse superior colliculus. J Neurosci. 2008; 28:11071–11078. [PubMed: 18945914]

Keilholz SD, Silva AC, Raman M, Merkle H, Koretsky AP. BOLD and CBV-weighted functional magnetic resonance imaging of the rat somatosensory system. Magn Reson Med. 2006; 55:316–324. [PubMed: 16372281]

Kim JP, Min HK, Knight EJ, Duffy PS, Abulseoud OA, Marsh MP, Kelsey K, Blaha CD, Bennet KE, Frye MA, Lee KH. Centromedian-parafascicular deep brain stimulation induces differential functional inhibition of the motor, associative, and limbic circuits in large animals. Biol Psychiatry. 2013a; 74:917–926. [PubMed: 23993641]

Kim SG, Harel N, Jin T, Kim T, Lee P, Zhao F. Cerebral blood volume MRI with intravascular superparamagnetic iron oxide nanoparticles. NMR Biomed. 2013b; 26:949–962. [PubMed: 23208650]

Knight EJ, Min HK, Hwang SC, Marsh MP, Paek S, Kim I, Felmlee JP, Abulseoud OA, Bennet KE, Frye MA, Lee KH. Nucleus accumbens deep brain stimulation results in insula and prefrontal activation: a large animal FMRI study. PLoS One. 2013; 8:e56640. [PubMed: 23441210]

Krautwald K, Angenstein F. Low frequency stimulation of the perforant pathway generates anesthesia-specific variations in neural activity and BOLD responses in the rat dentate gyrus. J Cereb Blood Flow Metab. 2012; 32:291–305. [PubMed: 21863039]

Kravitz AV, Freeze BS, Parker PR, Kay K, Thwin MT, Deisseroth K, Kreitzer AC. Regulation of parkinsonian motor behaviours by optogenetic control of basal ganglia circuitry. Nature. 2010; 466:622–626. [PubMed: 20613723]

Kringelbach ML, Jenkinson N, Owen SL, Aziz TZ. Translational principles of deep brain stimulation. Nat Rev Neurosci. 2007; 8:623–635. [PubMed: 17637800]

Lai HY, Albaugh DL, Kao YC, Younce JR, Shih YY. Robust deep brain stimulation functional MRI procedures in rats and mice using an MR-compatible tungsten microwire electrode. Magn Reson Med. 2015; 73:1246–1251. [PubMed: 24798216]

Lai HY, Younce JR, Albaugh DL, Kao YC, Shih YY. Functional MRI reveals frequency-dependent responses during deep brain stimulation at the subthalamic nucleus or internal globus pallidus. Neuroimage. 2014; 84:11–18. [PubMed: 23988274]

Lee JH, Durand R, Gradinaru V, Zhang F, Goshen I, Kim DS, Fenno LE, Ramakrishnan C, Deisseroth K. Global and local fMRI signals driven by neurons defined optogenetically by type and wiring. Nature. 2010; 465:788–792. [PubMed: 20473285]

Liu P, Basso MA. Substantia nigra stimulation influences monkey superior colliculus neuronal activity bilaterally. J Neurophysiol. 2008; 100:1098–1112. [PubMed: 18579662]

Lozano, Andres M., Lipsman, N. Probing and Regulating Dysfunctional Circuits Using Deep Brain Stimulation. Neuron. 2013; 77:406–424. [PubMed: 23395370]

MacLeod N, James T, Kilpatrick I, Starr M. Evidence for a GABAergic nigrothalamic pathway in the rat. Experimental Brain Research. 1980; 40:55–61. [PubMed: 6252030]

Magnuson M, Majeed W, Keilholz SD. Functional connectivity in blood oxygenation level-dependent and cerebral blood volume-weighted resting state functional magnetic resonance imaging in the rat brain. J Magn Reson Imaging. 2010; 32:584–592. [PubMed: 20815055]

Mallet N, Micklem BR, Henny P, Brown MT, Williams C, Bolam JP, Nakamura KC, Magill PJ. Dichotomous organization of the external globus pallidus. Neuron. 2012; 74:1075–1086. [PubMed: 22726837]

Michaelides M, Anderson SA, Ananth M, Smirnov D, Thanos PK, Neumaier JF, Wang GJ, Volkow ND, Hurd YL. Whole-brain circuit dissection in free-moving animals reveals cell-specific mesocorticolimbic networks. J Clin Invest. 2013; 123:5342–5350. [PubMed: 24231358]

Min HK, Hwang SC, Marsh MP, Kim I, Knight E, Striemer B, Felmlee JP, Welker KM, Blaha CD, Chang SY, Bennet KE, Lee KH. Deep brain stimulation induces BOLD activation in motor and non-motor networks: an fMRI comparison study of STN and EN/GPi DBS in large animals. Neuroimage. 2012; 63:1408–1420. [PubMed: 22967832]

Mishra AM, Ellens DJ, Schridde U, Motelow JE, Purcaro MJ, DeSalvo MN, Enev M, Sanganahalli BG, Hyder F, Blumenfeld H. Where fMRI and electrophysiology agree to disagree: corticothalamic and striatal activity patterns in the WAG/Rij rat. J Neurosci. 2011; 31:15053–15064. [PubMed: 22016539]

Moro E, Lozano AM, Pollak P, Agid Y, Rehncrona S, Volkmann J, Kulisevsky J, Obeso JA, Albanese A, Hariz MI, Quinn NP, Speelman JD, Benabid AL, Fraix V, Mendes A, Welter ML, Houeto JL, Cornu P, Dormont D, Tornqvist AL, Ekberg R, Schnitzler A, Timmermann L, Wojtecki L, Gironell A, Rodriguez-Oroz MC, Guridi J, Bentivoglio AR, Contarino MF, Romito L, Scerrati M, Janssens M, Lang AE. Long-term results of a multicenter study on subthalamic and pallidal stimulation in Parkinson's disease. Mov Disord. 2010; 25:578–586. [PubMed: 20213817]

Murphy K, Birn RM, Handwerker DA, Jones TB, Bandettini PA. The impact of global signal regression on resting state correlations: are anti-correlated networks introduced? Neuroimage. 2009; 44:893–905. [PubMed: 18976716]

Novak P, Klemp JA, Ridings LW, Lyons KE, Pahwa R, Nazzaro JM. Effect of deep brain stimulation of the subthalamic nucleus upon the contralateral subthalamic nucleus in Parkinson disease. Neurosci Lett. 2009; 463:12–16. [PubMed: 19616068]

Okun MS. Deep-brain stimulation for Parkinson's disease. N Engl J Med. 2012; 367:1529–1538. [PubMed: 23075179]

Paek SB, Min HK, Kim I, Knight EJ, Baek JJ, Bieber AJ, Lee KH, Chang SY. Frequency-dependent functional neuromodulatory effects on the motor network by ventral lateral thalamic deep brain stimulation in swine. Neuroimage. 2015; 105:181–188. [PubMed: 25451479]

Pawela CP, Biswal BB, Cho YR, Kao DS, Li R, Jones SR, Schulte ML, Matloub HS, Hudetz AG, Hyde JS. Resting-state functional connectivity of the rat brain. Magn Reson Med. 2008; 59:1021–1029. [PubMed: 18429028]

Paxinos, G., Watson, C. The rat brain in stereotaxic coordinates. 5. Academic Press; New York, NY: 2004.

Piedimonte F, Andreani JC, Piedimonte L, Graff P, Bacaro V, Micheli F, Vilela Filho O. Behavioral and motor improvement after deep brain stimulation of the globus pallidus externus in a case of Tourette's syndrome. Neuromodulation. 2013; 16:55–58. [PubMed: 23240689]

Raichle ME. The restless brain. Brain Connect. 2011; 1:3–12. [PubMed: 22432951]

Ross EK, Kim JP, Settell ML, Han SR, Blaha CD, Min HK, Lee KH. Fornix deep brain stimulation circuit effect is dependent on major excitatory transmission via the nucleus accumbens. Neuroimage. 2016; 128:138–148. [PubMed: 26780572]

Saunders A, Oldenburg IA, Berezovskii VK, Johnson CA, Kingery ND, Elliott HL, Xie T, Gerfen CR, Sabatini BL. A direct GABAergic output from the basal ganglia to frontal cortex. Nature. 2015; 521:85–89. [PubMed: 25739505]

Schmidt R, Leventhal DK, Mallet N, Chen F, Berke JD. Canceling actions involves a race between basal ganglia pathways. Nat Neurosci. 2013; 16:1118–1124. [PubMed: 23852117]

Shi LH, Luo F, Woodward D, Chang JY. Deep brain stimulation of the substantia nigra pars reticulata exerts long lasting suppression of amygdala-kindled seizures. Brain Res. 2006; 1090:202–207. [PubMed: 16647692]

Shih YY, Chen CC, Shyu BC, Lin ZJ, Chiang YC, Jaw FS, Chen YY, Chang C. A new scenario for negative functional magnetic resonance imaging signals: endogenous neurotransmission. J Neurosci. 2009; 29:3036–3044. [PubMed: 19279240]

Shih YY, Huang S, Chen YY, Lai HY, Kao YC, Du F, Hui ES, Duong TQ. Imaging neurovascular function and functional recovery after stroke in the rat striatum using forepaw stimulation. J Cereb Blood Flow Metab. 2014a; 34:1483–1492. [PubMed: 24917039]

Shih YY, Li G, Muir ER, De La Garza BH, Kiel JW, Duong TQ. Pharmacological MRI of the choroid and retina: blood flow and BOLD responses during nitroprusside infusion. Magn Reson Med. 2012; 68:1273–1278. [PubMed: 22183830]

Shih YY, Wang L, De La Garza BH, Li G, Cull G, Kiel JW, Duong TQ. Quantitative retinal and choroidal blood flow during light, dark adaptation and flicker light stimulation in rats using fluorescent microspheres. Curr Eye Res. 2013; 38:292–298. [PubMed: 23317112]

Shih YY, Wey HY, De La Garza BH, Duong TQ. Striatal and cortical BOLD, blood flow, blood volume, oxygen consumption, and glucose consumption changes in noxious forepaw electrical stimulation. J Cereb Blood Flow Metab. 2011; 31:832–841. [PubMed: 20940730]

Shih YY, Yash TV, Rogers B, Duong TQ. fMRI of deep brain stimulation at the rat ventral posteromedial thalamus. Brain Stimulation. 2014b; 7:190–193. [PubMed: 24309153]

Shyu BC, Lin CY, Sun JJ, Chen SL, Chang C. BOLD response to direct thalamic stimulation reveals a functional connection between the medial thalamus and the anterior cingulate cortex in the rat. Magn Reson Med. 2004; 52:47–55. [PubMed: 15236366]

Silva AC, Koretsky AP, Duyn JH. Functional MRI impulse response for BOLD and CBV contrast in rat somatosensory cortex. Magn Reson Med. 2007; 57:1110–1118. [PubMed: 17534912]

Takakusaki K, Saitoh K, Harada H, Okumura T, Sakamoto T. Evidence for a role of basal ganglia in the regulation of rapid eye movement sleep by electrical and chemical stimulation for the pedunculopontine tegmental nucleus and the substantia nigra pars reticulata in decerebrate cats. Neuroscience. 2004; 124:207–220. [PubMed: 14960352]

Tecuapetla F, Matias S, Dugue GP, Mainen ZF, Costa RM. Balanced activity in basal ganglia projection pathways is critical for contraversive movements. Nat Commun. 2014; 5:4315. [PubMed: 25002180]

Valdes-Hernandez PA, Sumiyoshi A, Nonaka H, Haga R, Aubert-Vasquez E, Ogawa T, Iturria-Medina Y, Riera JJ, Kawashima R. An in vivo MRI Template Set for Morphometry, Tissue Segmentation, and fMRI Localization in Rats. Front Neuroinform. 2011; 5:26. [PubMed: 22275894]

Velisek L, Veliskova J, Moshe SL. Electrical stimulation of substantia nigra pars reticulata is anticonvulsant in adult and young male rats. Exp Neurol. 2002; 173:145–152. [PubMed: 11771947]

Vitek JL, Hashimoto T, Peoples J, DeLong MR, Bakay RA. Acute stimulation in the external segment of the globus pallidus improves parkinsonian motor signs. Mov Disord. 2004; 19:907–915. [PubMed: 15300655]

Weiss D, Walach M, Meisner C, Fritz M, Scholten M, Breit S, Plewnia C, Bender B, Gharabaghi A, Wachter T, Kruger R. Nigral stimulation for resistant axial motor impairment in Parkinson's disease? A randomized controlled trial. Brain. 2013; 136:2098–2108. [PubMed: 23757762]

Wichmann T, Delong MR. Deep-Brain Stimulation for Basal Ganglia Disorders. Basal Ganglia. 2011; 1:65–77. [PubMed: 21804953]

Wille C, Steinhoff BJ, Altenmuller DM, Staack AM, Bilic S, Nikkhah G, Vesper J. Chronic high-frequency deep-brain stimulation in progressive myoclonic epilepsy in adulthood--report of five cases. Epilepsia. 2011; 52:489–496. [PubMed: 21219312]

Wu EX, Wong KK, Andrassy M, Tang H. High-resolution in vivo CBV mapping with MRI in wild-type mice. Magn Reson Med. 2003; 49:765–770. [PubMed: 12652549]

Yan CG, Craddock RC, Zuo XN, Zang YF, Milham MP. Standardizing the intrinsic brain: towards robust measurement of inter-individual variation in 1000 functional connectomes. Neuroimage. 2013; 80:246–262. [PubMed: 23631983]

Younce JR, Albaugh DL, Shih YY. Deep Brain Stimulation with Simultaneous fMRI in Rodents. J Vis Exp. 2014:e51271–e51271. [PubMed: 24561922]

Zhao F, Williams M, Meng X, Welsh DC, Grachev ID, Hargreaves R, Williams DS. Pain fMRI in rat cervical spinal cord: an echo planar imaging evaluation of sensitivity of BOLD and blood volume-weighted fMRI. Neuroimage. 2009; 44:349–362. [PubMed: 18835453]

Zhao F, Zhao T, Zhou L, Wu Q, Hu X. BOLD study of stimulation-induced neural activity and resting-state connectivity in medetomidine-sedated rat. Neuroimage. 2008; 39:248–260. [PubMed: 17904868]

Highlights

- fMRI during deep brain stimulation at striatal output nuclei (GPe and SNr)
- Robust cerebral blood volume increases in prefrontal cortex during GPe-DBS
- Bilateral striatal modulation by GPe and SNr-DBS
- Pathways showing frequency-dependent functional connectivity changes by GPe and SNr-DBS are identified

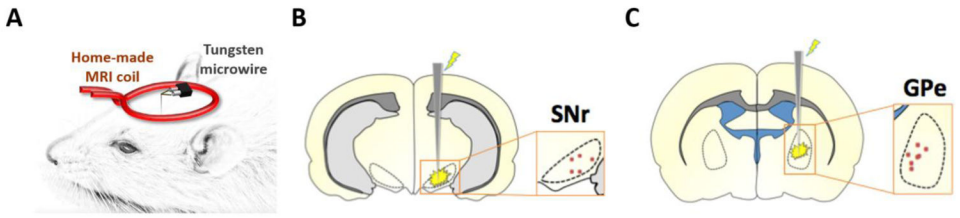

Figure 1.

(A) Schematic of the experimental setup, including custom surface coil and microwire DBS electrode. **(B–C)** Electrode tip placements within the SNr **(B)** and GPe **(C)** of all experimental subjects. Tip placements were estimated using T_2-weighted anatomical scans, which we deemed satisfactory given the relatively large size (including anteroposterior distance) of our targets, as well as the minimal electrode artifact.

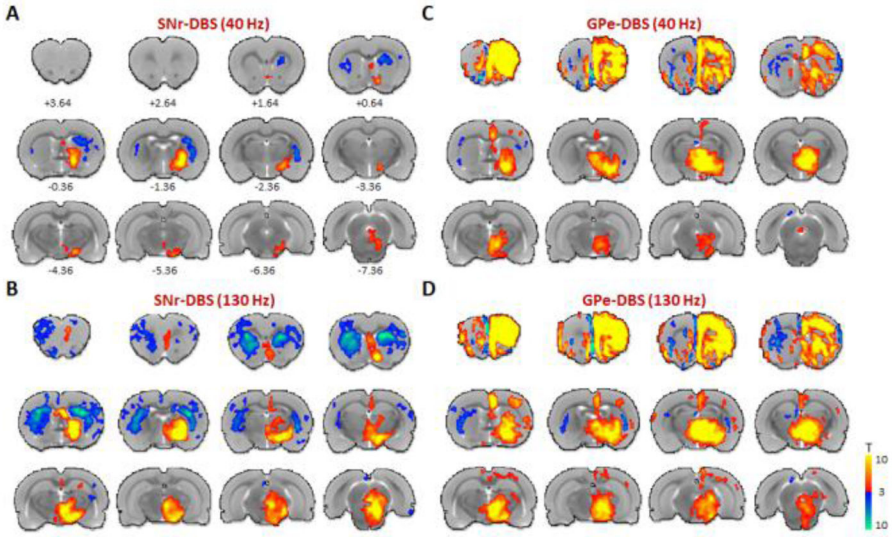

Figure 2.

Functional activation maps of CBV modulation by SNr- and GPe-DBS. Two DBS stimulation frequencies are shown for each target: SNr- DBS at 40 or 130 Hz **(A** and **B**, respectively), GPe-DBS at 40 or 130 Hz **(C** and **D**, respectively). Notable observations include CBV decreases in the striatum at both targets, as well as large, ipsilateral frontal cortical modulation by GPe-DBS. At both targets, stimulation responses were largely ipsilateral and stronger at 130 Hz compared to 40 Hz. 12 slices were acquired in each scan, with numbers below slices denoting relative distance from bregma (in mm). Color bar denotes t score values obtained by GLM analyses, with a significance threshold of $p < 0.05$. Functional activation maps for all additional tested frequencies are located in Supplemental Figures S4–5.

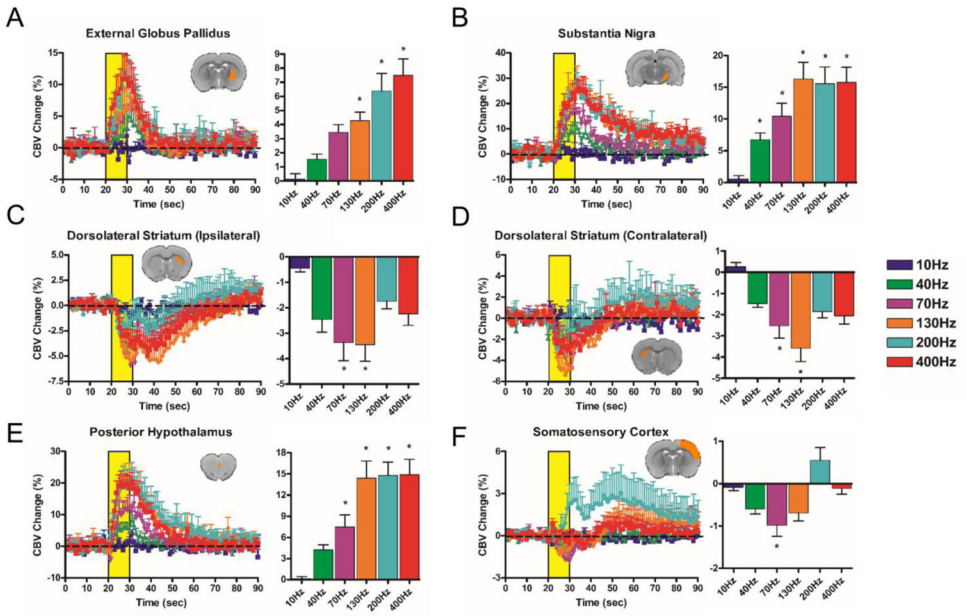

Figure 3.

SNr-DBS evoked CBV changes at select, anatomically-defined regions of interest. CBV traces (10–400 Hz; yellow bar denotes stimulation epoch; note different Y axis scales across ROIs) are accompanied by bar graphs displaying percent changes in CBV amplitude changes during the stimulation period (mean ± SEM CBV values for the DBS stimulation period). * denotes significant differences in CBV amplitude from 10 Hz ($p < 0.05$). Insert depicts representative slice example for each pre-defined ROI (note that most ROIs encompassed multiple slices). Unless otherwise denoted, all ROIs are ipsilateral to the DBS hemisphere. **(A)** External globus pallidus **(B)** Substantia nigra **(C)** Ipsilateral dorsolateral striatum **(D)** Contralateral dorsolateral striatum **(E)** Posterior hypothalamus **(F)** Somatosensory cortex. Additional ROIs (total = 19) are located in Supplemental Figure S6.

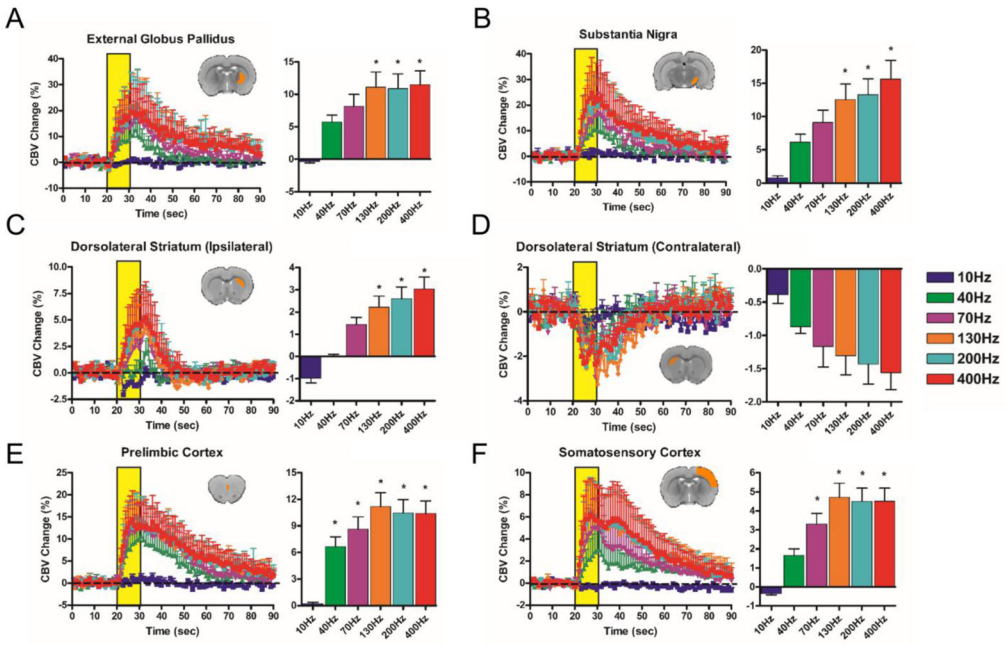

Figure 4.

GPe-DBS evoked CBV changes at select, anatomically-defined regions of interest. CBV traces (10–400 Hz; yellow bar denotes stimulation epoch; note different Y axis scales across ROIs) are accompanied by bar graphs displaying percent changes in CBV amplitude changes during the stimulation period (mean ± SEM CBV values for the DBS stimulation period). * denotes significant differences in CBV amplitude from 10 Hz ($p < 0.05$). Insert depicts representative slice example for each pre-defined ROI (note that most ROIs encompassed multiple slices). Unless otherwise stated, all ROIs are ipsilateral to the DBS hemisphere. **(A)** External globus pallidus **(B)** Substantia nigra **(C)** Ipsilateral dorsolateral striatum **(D)** Contralateral dorsolateral striatum **(E)** Prelimbic cortex **(F)** Somatosensory cortex. Note that the displayed ROI's for Panel E differ between Figures 3 and 4. Additional ROIs (total = 19; including Posterior hypothalamus) are located in Supplemental Figure S7.

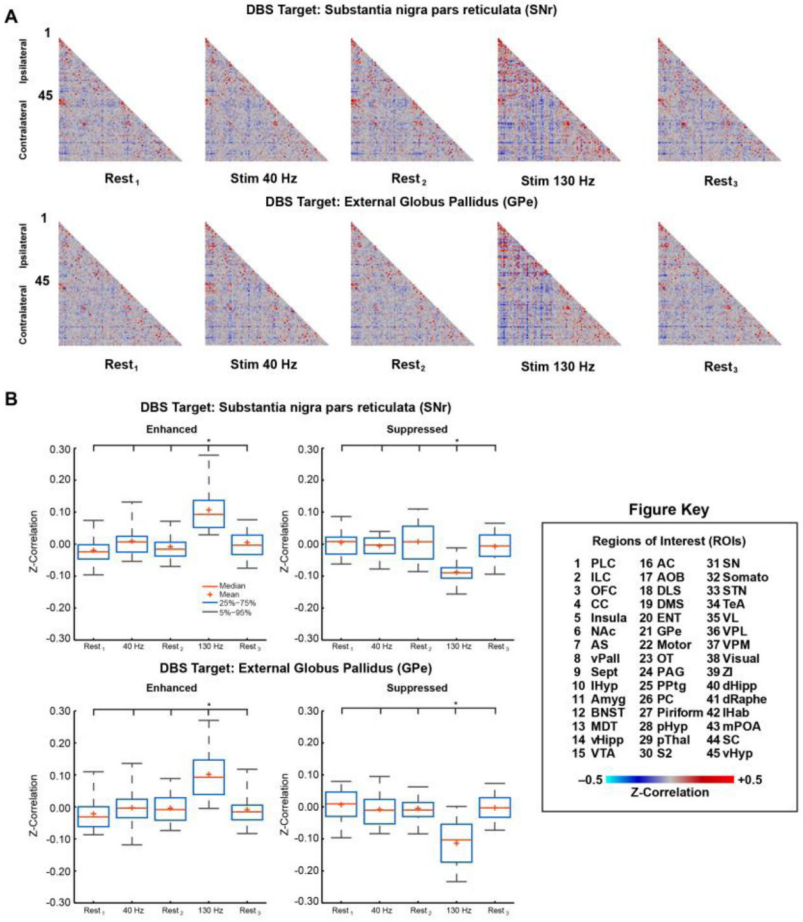

Figure 5.

fcMRI Modulation via DBS of the SNr and GPe. **(A)** Mean correlation matrices (SNr $n = 6$, GPe $n = 7$) for each stimulus condition ($Rest_1$, Stim 40 Hz, $Rest_2$, Stim 130 Hz, $Rest_3$) using 45 region-of-interests (ROIs: 1–45 Ipsilateral, 46–90 Contralateral, see Figure Key). **(B)** Post-hoc comparison of significantly modulated connections. Significance of individual connections (see Supporting Material: Supplemental Tables 1–2) was determined using repeated measures analysis of variance across animals (rANOVA, $p \leq 0.01$ uncorrected, $\Delta_{Z\text{-correlation}} \geq 0.10$). Connections were grouped according to modulation direction (Enhanced: increased correlation; Suppressed: increased anti-correlation) and then two-sample t-tests (see Supporting Material: Table S3) were used to statistically compare stimulus conditions (Rest, 40 Hz, and 130 Hz, see Figure Key). Data plotted as mean ± standard error of the mean (SEM). * denotes pair-wise significant ($p < 0.001$) differences. Abbreviations: **PLC**: Prelimbic Cortex; **ILC**: Infralimbic Cortex; **OFC**: Orbitofrontal Cortex; **CC**: Cingulate Cortex; **Insula**: Insular Cortex; **NAc**: Nucleus Accumbens; **AS**; Anterior Striatum; **vPAll**: Ventral Pallidum; **Sept**: Septum; **lHyp**: Lateral Hypothalamus; **Amyg**: Amygdala; **BNST**: Bed Nucleus of the Stria Terminalis; **MDT**: Mediodorsal Thalamus; **vHipp**: Ventral Hippocampus; **VTA**: Ventral Tegmental Area; **AC**: Auditory Cortex; **AOB**: Accessory Olfactory Bulb; **DLS**: Dorsolateral Striatum; **DMS**: Dorsomedial Striatum; **ENT**: Entorhinal Cortex; **GPe**: External Globus Pallidus; **Motor**: Motor Cortex

(Primary and Secondary); **OT**: Olfactory Tubercle; **PAG**: Periaqueductal Grey; **PPTg**: Pedunculopontine Tegmental Nucleus; **PC**: Parietal Cortex; **Piriform**: Piriform Cortex; **pHyp**: Posterior Hypothalamus; **pThal**: Posterior Thalamus; **S2**: Secondary Somatosensory Cortex; **SN**: Substantia Nigra; **Somato**: Primary Somatosensory Cortex; **STN**: Subthalamic Nucleus; **TeA:** Temporal Association Cortex; **VL**: Ventrolateral Thalamus; **VPL**: Ventral Posterolateral Thalamus; **Visual**: Visual Cortex (Primary and Secondary); **ZI**: Zona Incerta; **dHipp:** Dorsal Hippocampus; **dRaphe**: Dorsal Raphe Nucleus; **lHab**: Lateral Habenula; **mPOA**: Medial Preoptic Area; **SC**: Superior Colliculus; **vHyp**: Ventral Hypothalamus

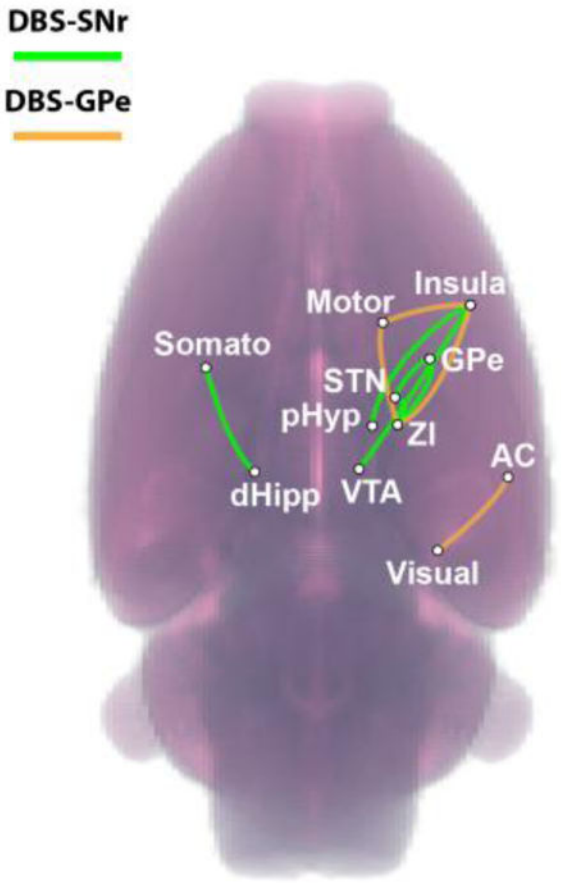

Figure 6.

Robust Functional Connectivity Modulation. Enhanced connections demonstrating more robust modulation (ΔZ-Corr > 0.20) overlaid on volume rendering of the rat brain (also see Tables S1–2). Green – SNr-DBS, Orange – GPe-DBS.